Assessment of anisotropic hardening models for conventional deep drawing processes

Originally published in:
International Journal of Material Forming 10(4), https://doi.org/10.1007/s12289-016-1306-7

Int J Mater Form (2017) 10:623–631
DOI 10.1007/s12289-016-1306-7

ORIGINAL RESEARCH

Assessment of anisotropic hardening models for conventional deep drawing processes

N. Manopulo[1] · **P. Peters**[1] · **P. Hora**[1]

Received: 5 August 2015 / Accepted: 21 June 2016 / Published online: 5 July 2016

Abstract Assessing the predictive capabilities of recent advanced constitutive modelling approaches for processes with industrial complexity is a challenging task. Real process conditions such as blankholder pressure distribution, friction and tool elasticity sensitively affect experimental observations, making the isolation of constitutive effects difficult. A systematic approach is proposed in this work to assess the performance of anisotropic hardening models with the least possible disturbance from process conditions. Two deep drawing examples were used for these purpose ("cross die" and "lackfrosch") in conjunction with a mild steel (DC05). Optically measured strain distributions have been compared to corresponding simulations, which have been calibrated to accurately match the measured blank draw-in. The effect of initial yield locus shape as well as anisotropic hardening effects have been discussed.

Keywords Constitutive modelling · Anisotropic hardening · HAH

Introduction

Numerical simulation of sheet metal forming processes is nowadays well established in industrial applications. Especially in automotive industry, the use of simulation technology has enabled the fast and efficient manufacturing of forming tools with unprecedented complexity. The appropriate modelling of forming materials is clearly one of the most important factors which led to the mentioned result. In fact the forming community has mostly concentrated efforts on the improved modelling of materials, successfully developing approaches to deal with the different plasticity effects observed in laboratory experiments. The central question remains whether the expected benefit from using complex constitutive approaches, is high enough to compensate for the additional experimental and computational cost required. Such a generic assessment is highly challenging if not impossible, given the infinite geometrical freedom encountered in sheet forming operations. The closest possible effort for this kind of approach is the Numisheet Benchmark organised every 3 years. However, as participants have the freedom of using different codes, it is not easy to recognize a clear correlation between advanced constitutive models and increased result accuracy (see e.g. [1]).

The present contribution aims reporting the results of a systematic analysis about the role of anisotropic hardening effects on the deep drawing of parts with industrial complexity. Firstly, it is demonstrated based on laboratory experiments that the considered material (DC05) exhibits significant anisotropy, non-proportional hardening, as well as Bauschinger effect (BE) and latent hardening. Recently proposed approaches are then used to accurately model the behaviour of these materials. The resulting models are implemented in LS-Dyna and computed strain distributions for two different geometries are validated against optical measurement results. To isolate the effect of material characterization, the remaining process complexities, especially friction coefficient and blankholder pressure, have been calibrated to obtain the best possible match between the simulated and experimental blank draw-in. More extensive information about the presented results can be found in the dissertation thesis of P. Peters [2].

✉ N. Manopulo
manopulo@ivp.mavt.ethz.ch

[1] ETH Zurich, Institute of Virtual Manufacturing, Tannenstrasse 3, 8092 Zurich, Switzerland

Anisotropic hardening effects

The inappropriate modelling of the material is usually counted as one of the primary sources of simulation inaccuracies. The isotropic hardening assumption, which can be proven to be inaccurate based on simple experiments, constitutes one of the most important topics in the metal forming community and several approaches have been proposed to loosen this restriction. Basically three different effects are considered:

1. Non-proportional hardening
2. Bauschinger Effect
3. Latent Effects

The first is related to changes in the anisotropy of a material even in case of proportional loading. This is mostly considered to be due to the strain dependent evolution of texture, which induces a different rate of hardening in dependence of the loading condition. A common approach in literature, which is used to account for this effect is the description of the yield locus shape in dependence of the equivalent plastic strain. Examples of such methods include [3–6].

The Bauschinger effect can be termed as the transient (or permanent) reduction of yield stress at load reversal, also usually accompanied by an increased hardening rate. It is mostly attributed to the release of dislocations stacked at the grain boundaries during initial deformation. BE is one of the best studied phenomena in the plasticity literature. Many modelling approaches exist to account for these effect, most of which base on the concept of kinematic hardening (see e.g. [7–10]), assuming the translation of the yield locus in stress space as a result of deformation. An alternative to the kinematic hardening approach has been proposed by Barlat et al. in 2011 which considers a distortion of the yield locus in the stress space as a consequence of deformation [11]. This approach delivers basically equivalent results to earlier models, with the additional advantage of being flexible in its usage with different anisotropic yield functions as well as the fact that its coefficients can be identified in a decoupled manner.

Latent hardening (or softening) effects are transient changes in the hardening behaviour of the material, which are exhibited at load path change. It is usually attributed to the fact that deformation in the active slip systems cause an increase in the dislocation density in non-active systems as well. Once load path change occurs, the latter can increase or decrease the resistance to dislocation movement on the newly activated systems, leading to a transient difference in the yield stress with respect to the monotonic behaviour. It can be for example observed in a two-step uniaxial tensile test, where the second deformation is conducted at a different angle than the first. For many materials this leads to a transient overshoot (latent hardening) or undershoot (cross loading contraction) of the monotonic yield stress. This kind of behaviour has been reported in many publications (e.g. [11–16]). Dislocation density based models (e.g. [17, 18]) as well as kinematic hardening based models accounting for dislocation structures, have been proposed in this context (e.g. [14, 19]). Barlat et al. extended their original application in two recent publications [20, 21], where they proposed a simple and effective way of considering latent effects using a distortional hardening approach. A thorough analysis of the latter can be found in [22].

Material properties

The investigations detailed in the present work, have been carried out using a deep drawing quality steel (DC05). Tensile tests in different directions, bulge tests, stack compression tests, two-step uniaxial tension tests as well as cyclic shear tests have been carried out to fully characterize the material. The experimental results as well as the calibrated material models will be illustrated in this section.

Flow curves and yield locus

The flow curves in 0, 45 and 90° to rolling direction as well as the measured equibiaxial flow curve can be seen in Fig. 1.

These deliver all the necessary input quantities for characterizing the yld2000-2d [23] model, except for the biaxial r-value which has been measured with a stack compression test. The mechanical parameters measured and the resulting yield locus parameters are given in Table 1.

The model is summarized in section 2.1.1 for ease of reference.

The YLD2000-2D model

The yield criterion according to the yld2000-2d formulation is given as:

$$\Phi = \left|X_1^{'} - X_2^{'}\right|^a + \left|2X_2^{''} + X_1^{''}\right|^a + \left|2X_1^{''} + X_2^{''}\right|^a = 2\overline{\sigma}^a$$

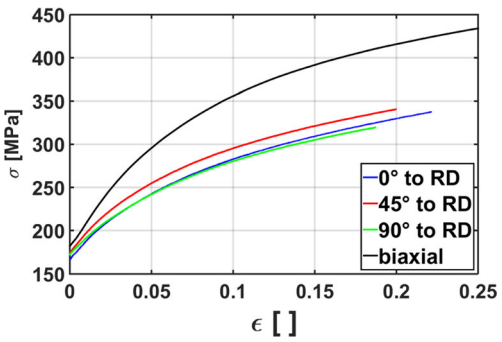

Fig. 1 Flow curves DC05

Table 1 Mechanical properties and corresponding yield locus parameters for yld2000-2d (DC05). The yield locus exponent is taken as a = 6

σ_0	σ_{45}	σ_{90}	σ_b	r_0	r_{45}	r_{90}	r_b
171	178	177	195	2.00	1.47	2.52	0.85
α_1	α_2	α_3	α_4	α_5	α_6	α_7	α_8
1.08	0.98	0.85	0.88	0.91	0.84	0.97	0.98

Here, $\overline{\sigma}$ is the equivalent stress, a is the material exponent and $X_1^{'}$, $X_2^{'}$, $X_1^{''}$ and $X_2^{''}$ are the principal values of two linear transformations of the stress deviator defined as:

$$\boldsymbol{X}^{'} = \boldsymbol{C}^{'}\boldsymbol{s} = \boldsymbol{C}^{'}\boldsymbol{T}\boldsymbol{\sigma} = \boldsymbol{L}^{'}\boldsymbol{\sigma}$$
$$\boldsymbol{X}^{''} = \boldsymbol{C}^{''}\boldsymbol{s} = \boldsymbol{C}^{''}\boldsymbol{T}\boldsymbol{\sigma} = \boldsymbol{L}^{''}\boldsymbol{\sigma}$$

with

$$L_{11}^{'} = \frac{2}{3}\alpha_1 \qquad L_{11}^{''} = \frac{-2\alpha_3 + 2\alpha_4 + 8\alpha_5 - 2\alpha_6}{9}$$
$$L_{12}^{'} = -\frac{1}{3}\alpha_1 \qquad L_{12}^{''} = \frac{\alpha_3 - 4\alpha_4 - 4\alpha_5 + 4\alpha_6}{9}$$
$$L_{21}^{'} = -\frac{1}{3}\alpha_2 \qquad L_{21}^{''} = \frac{4\alpha_3 - 4\alpha_4 - 4\alpha_5 + \alpha_6}{9}$$
$$L_{22}^{'} = \frac{2}{3}\alpha_2 \qquad L_{22}^{''} = \frac{-2\alpha_3 + 8\alpha_4 + 2\alpha_5 - 2\alpha_6}{9}$$
$$L_{33}^{'} = \alpha_7 \qquad L_{33}^{''} = \alpha_8$$

The model thus features eight independent parameters α_i which need to be identified based on the initial yield stresses σ_{y0}, σ_{y45}, σ_{y90} and the Lankford parameters r_0, r_{45}, r_{90} in 0°, 45° and 90° as well as the biaxial yield stress σ_{yb} and r_b which is defined by $r_b = \Delta\varepsilon_{yy}/\Delta\varepsilon_{xx}$.

Non-proportional hardening

Figure 4 depicts one-element simulation results conducted with LS-Dyna using the identified yld2000-2d model under equibiaxial loading. The isotropic hardening approach clearly underestimates the yield stress at larger strains. This occurs due to the fact that the biaxial configuration exhibits a stronger hardening rate than the tensile configurations, an effect which cannot be captured by isotropic hardening.

In order to account for this effect, the α parameters of the yld2000-2d model have been defined in dependence of the equivalent plastic strain, thus enabling a distortion of the yield locus. The critical issue in doing this, is selecting the appropriate stress values for a given equivalent plastic strain level, without infracting the fundamental requirement that yield locus contours represent levels of equivalent plastic work. This is done by computing an intermediate plastic work variable (see [6] and [24] for details). Figure 2 depicts the evolution of the yield locus, considering isotropic and anisotropic hardening approaches. It is noted that the equibiaxial stress point

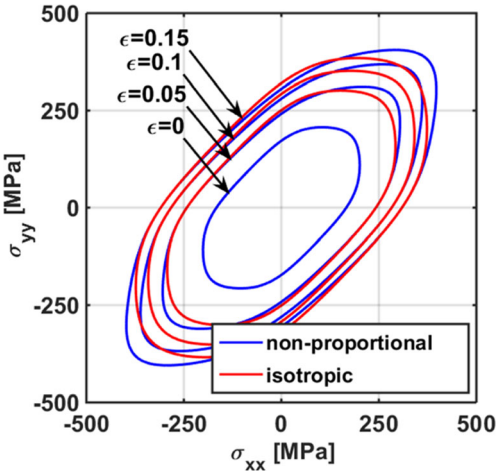

Fig. 2 Yield Locus shapes for different hardening models [6]

significantly differs between the two. The resulting evolution of the α parameters is depicted in Fig. 3.

This approach has been implemented in LS-Dyna as a UMAT subroutine, extending the Closest Point Projection algorithm described in [25] to accommodate a strain dependent evolution of the yield locus.

A simulation of the experimental paths with this algorithm delivered a much better match with the experiments as it can be seen in Fig. 4.

Bauschinger effect

In the context of deep drawing applicatons, the Bauschinger Effect (BE) plays a sensitive role on elastic springback, as the latter strongly depends on the local yield stress. Further situations where this effect can play a role are for example bending-unbending deformations as encountered in drawbeads or around die radii. In this work the HAH model [11, 12] has been used to investigate the role of BE on deep drawing applications.

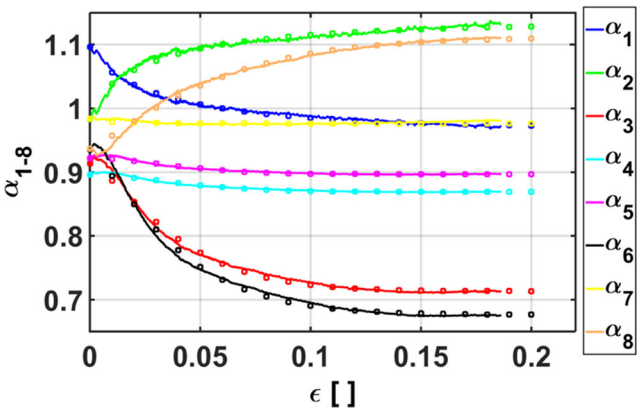

Fig. 3 Variable α parameters for yld2000-2d_var. The squares indicate a smooth approximation of the data based on the Hockett-Sherby model [6]

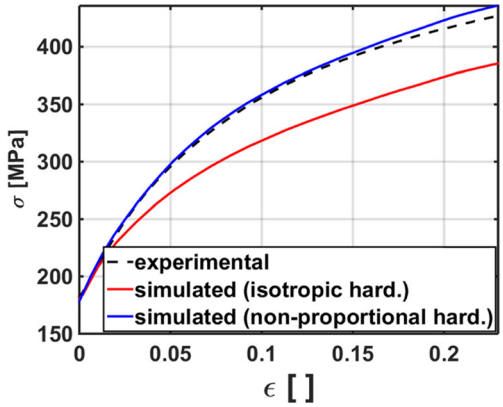

Fig. 4 Equibiaxial flow curves for DC05 with isotropic and non-proportional hardening models

The HAH model

The HAH model [11, 12] reads:

$$\overline{\sigma} = \left\{\phi^a + \phi_h^a\right\}^{1/a}$$

It is composed of a stable component ϕ, which is any homogeneous orthotropic yield locus description and a homogeneous component formulated as follows:

$$\phi_h = f_1|\xi - |\xi|| + f_2|\xi + |\xi||$$

Where $\xi = \hat{\mathbf{h}}^{\mathbf{s}} : \mathbf{s}$ with $\mathbf{s}$ the deviatoric part of the stress tensor and $\hat{\mathbf{h}}^{\mathbf{s}}$ the so-called microstructure deviator defined as:

$$\hat{\mathbf{h}}^{\mathbf{s}} = \frac{\mathbf{h}^{\mathbf{s}}}{\sqrt{\frac{8}{3}\mathbf{h}^{\mathbf{s}} : \mathbf{h}^{\mathbf{s}}}}$$

Barlat et al. suggest to initialize the tensor $\mathbf{h}^{\mathbf{s}}$ to be equal to the deviatoric stress tensor at the moment of the first plastic deformation, it can be then evolved depending on the equivalent plastic strain. The functions f_1 and f_2 depend in turn on two

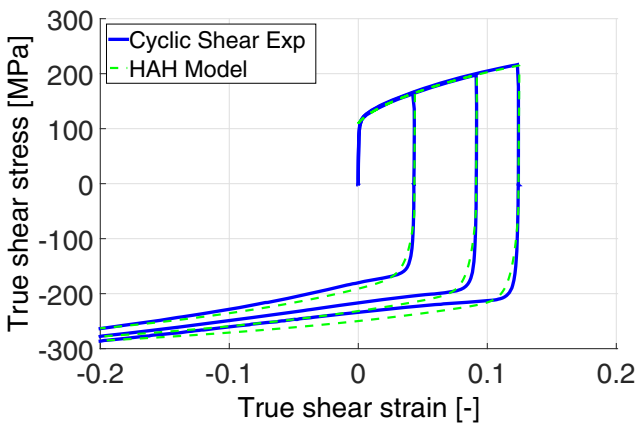

Fig. 5 Reverse shear experiments and HAH fit

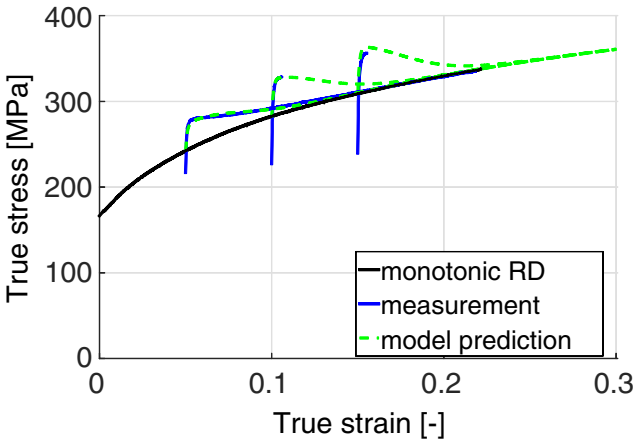

Fig. 6 Two step tensile tests with pre-strain in 45° followed by uniaxial tension in the rolling direction

state variables g_1 and g_2 describing the ratio of the distorted deviatoric stress to the isotropic case, in the following manner:

$$f_i = \left(g_i^{-q} - 1\right)^{1/q} \; i = 1, 2$$

For the case of no permanent softening Barlat et al. suggest the following evolution equations for the mentioned variables:

$$\text{if } \hat{\mathbf{h}}^{\mathbf{s}} : \mathbf{s} \geq 0 \qquad \text{if } \hat{\mathbf{h}}^{\mathbf{s}} : \mathbf{s} < 0$$

$$\frac{dg_1}{d\overline{\epsilon}} = k_2\left(k_3\frac{H_0}{H} - g_1\right) \qquad \frac{dg_1}{d\overline{\epsilon}} = k_1\left(\frac{1-g_1}{g_1}\right)$$

$$\frac{dg_2}{d\overline{\epsilon}} = k_1\left(\frac{1-g_2}{g_2}\right) \qquad \frac{dg_2}{d\overline{\epsilon}} = k_2\left(k_3\frac{H_0}{H} - g_2\right)$$

$$\frac{d\hat{\mathbf{h}}^{\mathbf{s}}}{d\overline{\epsilon}} = k\left(\hat{\mathbf{s}} - \frac{8}{3}\hat{\mathbf{h}}^{\mathbf{s}}\left(\hat{\mathbf{h}}^{\mathbf{s}} : \hat{\mathbf{s}}\right)\right) \qquad \frac{d\hat{\mathbf{h}}^{\mathbf{s}}}{d\overline{\epsilon}} = -k\left(\hat{\mathbf{s}} - \frac{8}{3}\hat{\mathbf{h}}^{\mathbf{s}}\left(\hat{\mathbf{h}}^{\mathbf{s}} : \hat{\mathbf{s}}\right)\right)$$

where k_i are model parameters. Cyclic shear tests have been carried out with the DC05 material, based on which the model parameters have been identified as follows:

k	k_1	k_2	k_3	k_4	k_5
28	158.4	6.3	0.1	0.9	10

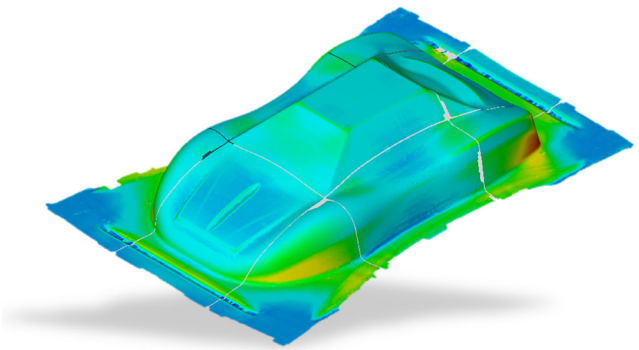

Fig. 7 Strain distribution measured with DIC (lackfrosch, AUDI AG)

Figure 5 depicts the flow curves derived from the cyclic shear experiments, as well as the approximation obtained with the HAH model.

It is seen that the model captures both early re-yielding and increased hardening rate quite well, it lacks however freedom to approximate the transient hardening stagnation. This effect can also be captured if a dislocation density based model is used, but was left out of the scope of this work.

Latent effects

Non-proportional loading is often encountered in deep drawing applications. This is especially the case for multi-stage forming processes. However nonlinear strain paths can very well occur also in single stage forming applications. An example is the drawing of a material point under the blank holder towards the die clearance where it switches from a tension-compression state towards a plane strain state. These phenomenon is often critical as immediate failure may occur.

Cross loading and latent hardening effects

A recent publication by Barlat et al. [20] also investigated the cross loading effects on the evolution of the yield locus. A new state variable g_L has been introduced in that publication to account for latent effects which then modifies the flow stress as follows:

$$\sigma_y = g_L H$$

The evolution equation for the latter is suggested in the same paper:

$$\frac{dg_L}{d\bar{\epsilon}} = k_L\left[\left(\frac{H-H_0}{H}\right)\left(\sqrt{L(1-\cos^2\chi)\ +\ \cos^2\chi}-1\right)+1-g_L\right]$$

where L is the latent hardening coefficient and k_L an additional coefficient for the evolution equation. The quantity $\cos\chi$ is an indicator for path change and is computed as

$$\cos\chi = \frac{8}{3}\,\hat{\mathbf{h}}^{\mathbf{s}} : \hat{\mathbf{s}}$$

In order to investigate the latent hardening behaviour of the DC05 material, two step uniaxial tensile tests have been carried out, where the material has been pre-stretched in different directions and then drawn in RD until failure. Figure 6 exemplarily shows the curves for pre-strain in 45°, where the typical stress overshoot due to latent hardening can be observed.

The extended HAH model [20] has been identified based on these experiments to have the following parameter values:

k_L	L
1600	1.86

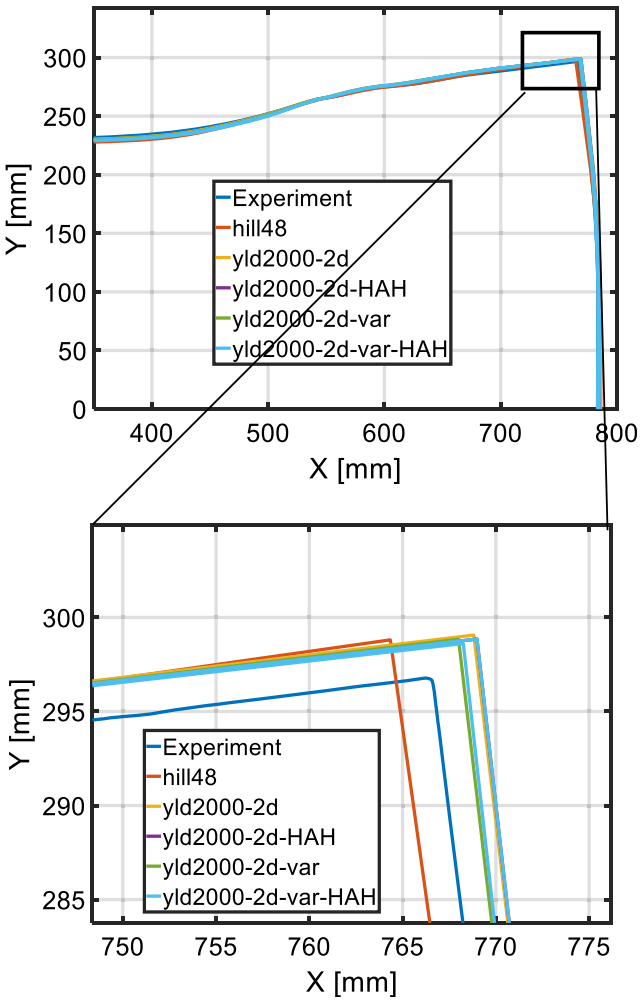

Fig. 8 Comparison of simulated and experimental draw-in (upper rigth quarter of the geometry in Fig. 7)

Again looking to Fig. 6 it is seen that the model is very well able of capturing this effect.

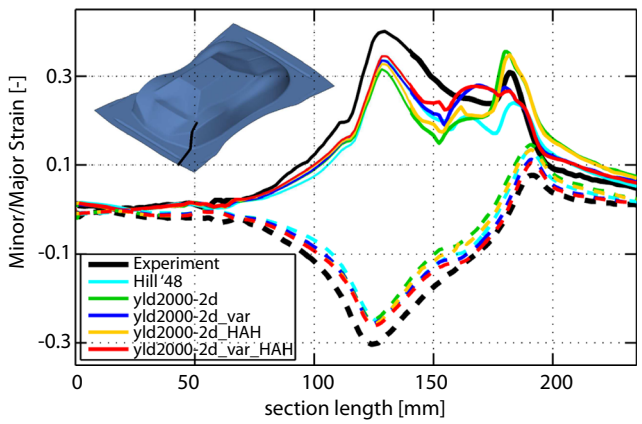

Fig. 9 Prediction of strains along a representative section of the cross-die (var. refers to the non-proportional hardening model with variable α -parameters)

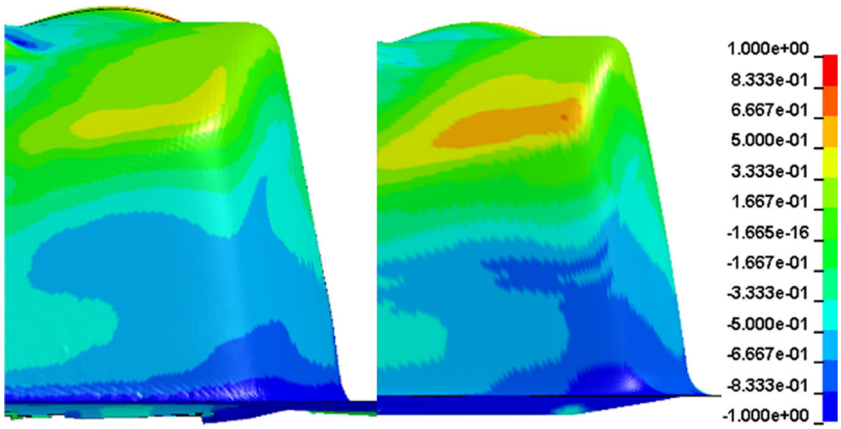

Fig. 10 Comparison between measured (left) and simulated (yld2000-2d) (right) strain ratios (ϵ_2/ϵ_1) in a view containing the representative section of Fig. 9

Deep drawing applications

The models considered in the previous section deliver accurate approximations of the different effects considered. The next question is whether these advanced models also enable an improvement in the prediction of strain distributions in deep drawing applications.

Two deep drawing geometries have been considered for the comparison, the "lackfrosch" geometry, provided by AUDI AG, and the "cross-die" geometry. Deep drawing experiments have been carried out with the materials and the resulting strain distribution has been measured using the ARGUS system from the company GOM mbH.

For the simulations the commercial explicit FE-code LS-Dyna has been used by implementing the mentioned models as user subroutines. The multi-stage cutting plane projection algorithm (CPP) has been extended for this purpose, to accommodate the strain dependent evolution of the yield locus. Belytchko-Tsay shell elements with 5 integration points across the thickness direction have been used with converged mesh density.

Lackfrosch geometry

The "lackfrosch" geometry used (Fig. 7), aims to mimic the geometry of a full car body and contains many of the loading conditions encountered in deep drawing applications.

The simulations have been calibrated for friction and blankholder force, to best fit the measured draw-in. The simple Coulomb friction model was used. The obtained parameter values are as follows:

Friction coeff. [−]	Blankholder Force [kN]
0.07	600

Note that only the base model (yld2000-2d) has been used to calibrate the draw-in. The rationale behind this choice is to find a good compromise between isolation of the material model and investigation of the constitutive effects. In fact changes in the material model can be expected to slightly affect the draw-in (see Fig. 8), which also plays a role in the overall accuracy reached. A calibration for each model would exclude this effect and thus lead to an unfair comparison.

Glancing at the strain distributions along a critical section (Fig. 9), it can be said the material models react sensitively. Both non-proportional loading and HAH models positively contribute to the predicted major strains. This can be attributed partially to the presence of drawbeads and also to the path non-linearity occuring around the die edge at the considered section.

Analysing the strain ratio distributions (Fig. 10) it is seen that a relatively good match of the strain state exists between measured and simulated results.

On the whole, however, the improvement provided by the complex modelling techniques is still not able of closing the gap between simulated and measured curves.

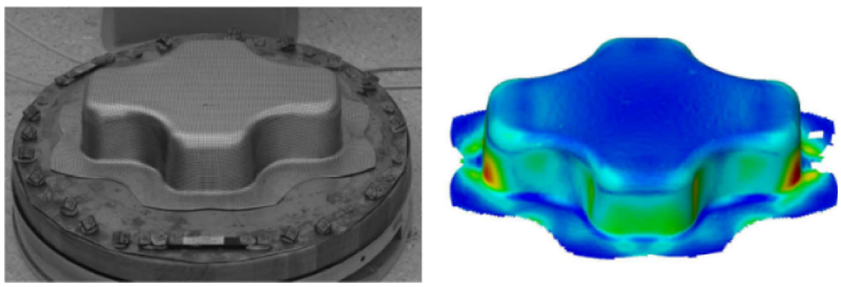

Fig. 11 Cross-die specimen (*left*). Strain distribution measured with DIC (*right*)

Cross-die geometry

The cross-die geometry (see Fig. 11) is used in many deep-drawing investigations as it is a good representative of many different stress and deformation states occurring in deep drawing applications.

Again, the simulations have been calibrated using only the yld2000-2d model, to obtain the best possible match in the predicted blank draw-in. The obtained parameter values are as follows:

Friction coeff. [−]	Blankholder Force [kN]
0.08	200

Figure 12 depicts a comparison of the predicted and measured blank outlines for all different model combinations. All yld2000-2d based models show good accordance although the model has been calibrated uisng only the basic version of the model. Hill48 shows the largest deviations.

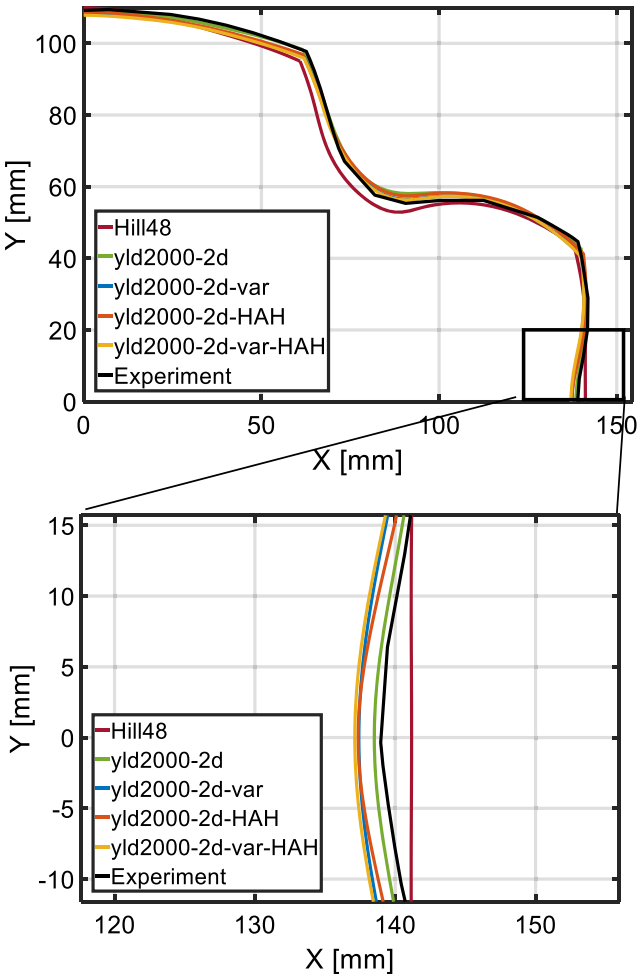

Fig. 12 Comparison of simulated and experimental draw-in for the different models (upper right quarter of the geometry in Fig. 11)

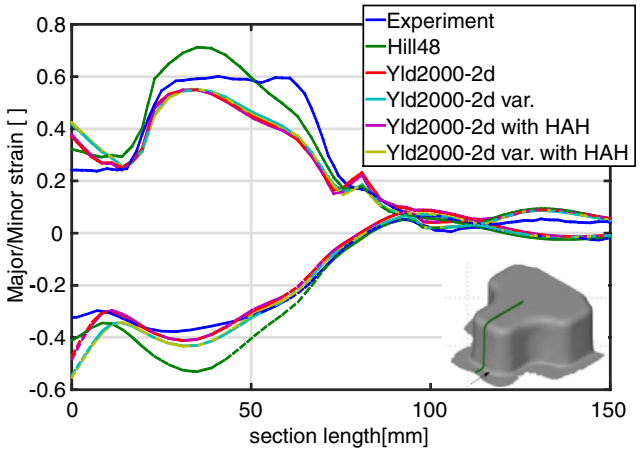

Fig. 13 Prediction of strains along a representative section of the cross-die. (var. refers to the non-proportional hardening model with variable α -parameters)

The results obtained using the different modelling approaches are compared along a representative section (see Fig. 13). It can be observed that the effect of the chosen yield locus model is in this case significantly larger than the effect of anisotropic hardening. The Hill48 model [26], which can be seen as an industry standard for deep drawing steels, overshoots the strains in the lower half of the wall and underestimates them in the upper half. The yld2000-2d model on the other hand gets fairly close to the measured strains in the lower half, but clearly underestimates them in the upper half. No significant influence of Bauschinger effect or latent hardening is observed.

It could be argued at this point that the path nonlinearity along the considered section might be insignificant. Figure 14 depicts the computed strain ratio history versus the punch depth for two extremal points selected on the wall along the section.

Especially for the element near the die radius, the strain ratio of which changes between uniaxial and plane strain

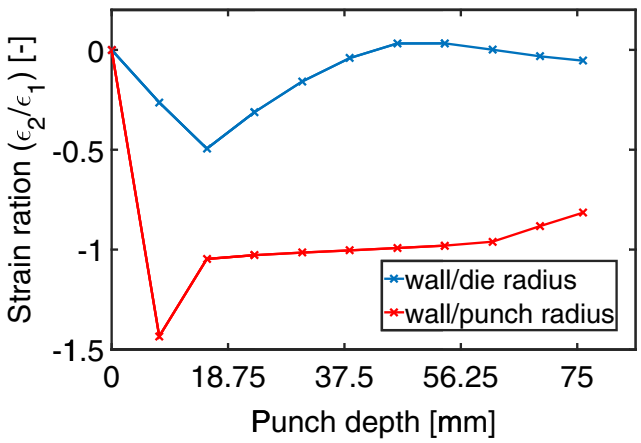

Fig. 14 Strain ratio history of two elements selected on the representative section

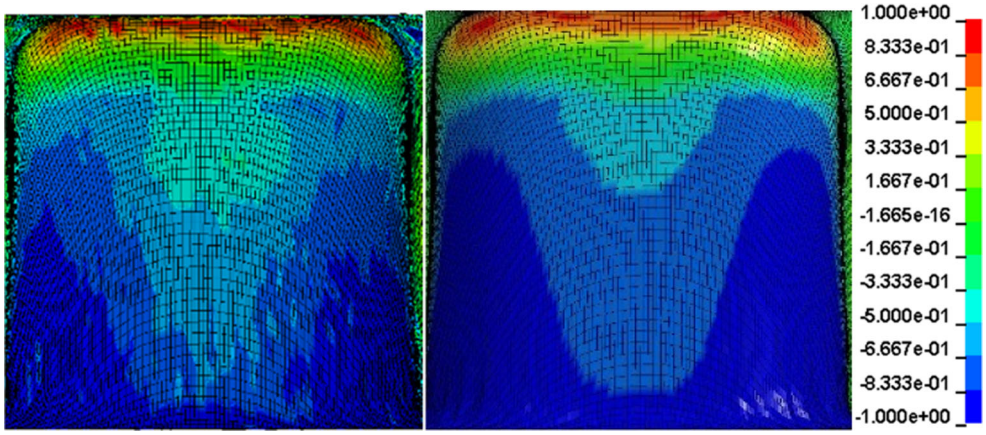

Fig. 15 Comparison between measured (*left*) and simulated (yld2000-2d) (*right*) strain ratios (ϵ_2/ϵ_1) in a view containing the representative section of Fig. 13

tension, a significant nonlinearity in the deformation path is observed.

Figure 15 shows a comparison between strain ratios projected on the considered geometry. In the lower portion of the wall, it is seen that the simulated strain ratios (and consequently stress ratios) less accurately match measured ones. On the other hand, it is seen that the top portion of the wall, where a stress state between plane strain and equibiaxial tension occurs, is simulated quite accurately. As anisotropic hardening is most strongly exhibited in equibiaxial tension, it can be expected that advanced models deliver a better approximation in this region. This is confirmed by zooming in Fig. 13 to the range between 80 and 120 mm (Fig. 16), which roughly corresponds to the said region.

In fact it is seen that the yld2000-2d model with variable α -parameters very closely matches the strains here and the isotropic hardening model remains inaccurate. No significant influence of path nonlinearity is observed. It is noted that the overall magnitude of the strains is very low here, so the benefit obtained by advanced modelling remains secondary with respect to the larger deviations observed in high strain regions.

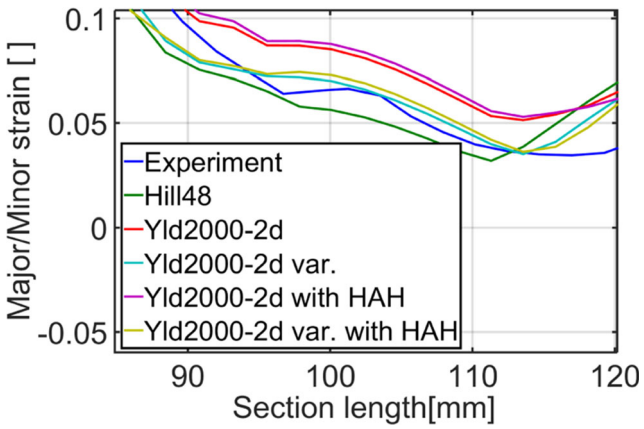

Fig. 16 Zoomed view of Fig. 13 depicting the region roughly around the punch radius. (var. refers to the non-proportional hardening model with variable α -parameters)

Conclusions

The objective of this contribution is to propose a systematic methodology to assess advanced material models in presence of complex loading conditions arising in realistic deep drawing processes.

The following conclusions can be drawn from the analysis:

- The chosen material modelling approach is a very significant factor in the accuracy level of deep drawing simulations.
- For the considered geometries it is seen that the description of the initial yield locus, reacts most sensitively on the obtained results, followed by non-proportional hardening effects and to a lesser extent by Bauschinger and Latent hardening effects. This is mainly because the regions sensitively reacting to anisotropic hardening feature relatively low deformation.
- The effect of contact and friction under the blankholder has been minimized by calibrating the blank draw-in based on experimental evidence. The contact and friction condition around the die and punch radii can however still be decisive in the obtained loading condition. More research in this direction is necessary.

In order to keep the focus on material modelling all other process aspects have been modelled using standard, industrially well accepted methods. This does not imply that the used approaches are accurate enough to fully describe the problem at hand. The objective of this choice is to provide results using models for which extensive experience exists, both in scientific and in industrial communities. The following points have

been thus let out of the scope of this work and can be suggested as future work in this direction:

- The finite elements used are based on a simplified shell element formulation. More sophisticated shell formulations (e.g. Hughes-Liu) or even 3D brick elements may be used at the cost of additional computational effort.
- The friction condition in deep drawing applications is known to be dependent on pressure, velocity and temperature. These dependencies can be costly to measure but also provide significant improvements in the modelling accuracy

Acknowledgements This work was carried out in the framework of the CTI (Commission for Technology and Innovation, Swiss Federation) project 10929.1 PFIW-IW. The financial support of the CTI is here gratefully acknowledged. Moreover, the authors thank AUDI AG for providing the "lackfrosch" geometry and experiments. Furthermore, the authors thank GOM mbH for assisting with the optical measurements. Finally, the UTG institute in TU München is thankfully acknowledged for their help in conducting the cross-die experiments.

Compliance with ethical standards

Funding This study was partly funded by the Commission for Technology and Innovation, Swiss Federation (grant number CTI10929.1 PFIW-IW).

Conflict of interest The authors declare that they have no conflict of interest.

References

1. Numisheet (2014) The 9th International Conference and Workshop on Numerical Simulation of 3D Sheet Metal Forming Processes, Part A: Benchmark Problems and results. AIP Conference Proceedings, Volume 1567, NUMISHEET 2014
2. Peters P Yield functions taking into account anisotropic hardening effects for an improved virtual representation of deep drawing processes, PhD thesis ETH Nr. 22707.
3. Suh YS, Saunders FI, Wagoner RH (1996) Anisotropic yield functions with plastic-strain-induced anisotropy. Int J Plast 12(3):417–438. doi:10.1016/S0749-6419(96)00014-9
4. Hora P, Hochholdinger B, Mutrux A and Tong L Modeling of anisoptropic hardening behavior based on Barlat 2000 yield locus description. In: Proceedings of the 3rd Forming Technology Forum Zurich 2009, pages 21–29, Zürich, 2009. Institute of Virtual Manufacturing
5. Wang H, Wan M, Wu X, Yan Y (2009) The equivalent plastic strain dependent yld2000-2d yield function and the experimental verification. Comput Mater Sci 47(1):12–22
6. Peters P, Manopulo N, Lange C, Hora P (2014) A strain rate dependent anisotropic hardening model and its validation through deep drawing experiments. Int J Mater Form 7(4):447–457
7. Prager W (1955) A new method of analyzing stresses and strains in workhardening plastic solids. Division of Applied Mathematics, Brown University
8. Armstrong PJ, Frederick C and Britain G (1966) A mathematical representation of the multiaxial Bauschinger effect. Central Electricity Generating Board [and] Berkeley Nuclear Laboratories, Research & Development Department
9. Chaboche J-L (1989) Constitutive equations for cyclic plasticity and cyclic viscoplasticity. Int J Plast 3:247–302
10. Yoshida F, Uemori T (2002) A model of large-strain cyclic plasticity describing the Bauschinger effect and work hardening stagnation. Int J Plast 18(5):661–686
11. Barlat F, Gracio JJ, Lee M-G, Rauch EF, Vincze G (2011) An alternative to kinematic hardening in classical plasticity. Int J Plast 27(9):1309–1327
12. Kim KH, Yin JJ (1997) Evolution of anisotropy under plane stress. J Mech Phys Solids 45:841–851
13. Raphanel JL, Schmitt J-H, Baudelet B (1989) Effect of a prestrain on the subsequent yielding of low carbon steel sheets: experiments and simulations. Int J Plast 2:371–378
14. Hu Z, Rauch EF, Teodosiu C (1992) Work-hardening behavior of mild steel under stress reversal at large strains. Int J Plast 8:839–856
15. Lopes AB, Barlat F, Gracio JJ, Ferreira Duarte J, Rauch EF (2003) Effect of texture and microstructure on strain hardening anisotropy for aluminum deformed in uniaxial tension and simple shear. Int J Plast 19:1–22
16. Barlat F, Ferreira Duarte J, Gracio JJ, Lopes AB, Rauch EF (2003) Plastic flow for non-monotonic loading conditions of an aluminum alloy sheet sample. Int J Plast 19:1215–1244
17. Rauch EF, Gracio JJ, Barlat F (2007) Work-hardening model for polycrystalline metals under strain reversal at large strains. Acta Mater 55:2939–2948
18. Rauch EF, Gracio JJ, Barlat F, Vincze G (2011) Modelling the plastic behaviour of metals under complex loading conditions. Model Simul Mater Sci Eng 19:035009 **(18 pp)**
19. Teodosiu C, Hu Z (1998) Microstructure in the continuum modeling of plastic anisotropy. In: Cartensen JV, Leffers T, Lorentzen T, Pedersen OB, Sørensen BF, Winther G (eds) Proc. Risø International Symposium on Material Science. Modelling of structure and mechanics of materials from microscale to products. Risø National Laboratory, Roskilde, Denmark, pp 149–168
20. Barlat F, Ha JJ, Gracio JJ, Lee MG, Rauch EF, Vincze G (2013) Extension of homogeneous anisotropic hardening model to cross loading with latent effects. Int J Plast 46:130–142. doi:10.1016/j.ijplas.2012.07.002
21. Barlat F, Vincze G, Grácio JJ, Lee M-G, Rauch EF, Tomé CN (2014) Enhancements of homogenous anisotropic hardening model and application to mild and dual-phase steels. Int J Plast 58:201–218. doi:10.1016/j.ijplas.2013.11.002
22. Manopulo N, Barlat F, Hora P (2015) Isotropic to distortional hardening transition in metal plasticity. Int J Solids Struct 56–57:11–19. doi:10.1016/j.ijsolstr.2014.12.015
23. Barlat F, Brem J, Yoon J, Chung K, Dick R, Lege D, Pourboghrat F, Choi S-H, Chu E (2003) Plane stress yield function for aluminum alloy sheets - part 1: theory. Int J Plast 19(9):1297–1319
24. Peters P, Leppin C and Hora P (2011) Method for the evaluation of the hydraulic bulge test. In Proceedings of IDDRG 2011. International Deep Drawing Research Group
25. Yoon J-W, Barlat F, Dick RE, Chung K, Kang TJ (2004) Plane stress yield function for aluminum alloy sheets - part II: FE formulation and its implementation. Int J Plast 20(3):495–522
26. Hill R (1948) A theory of the yielding and plastic flow of anisotropic metals. Proc R Soc Lond A Math Phys Sci 193(1033):281–297